PAPER

Check for updates

Conjugated microporous polymers using a copper-catalyzed [4 + 2] cyclobenzannulation reaction: promising materials for iodine and dye adsorption†

Noorullah Baig, [a,b] Suchetha Shetty, [a,b] Saleh Al-Mousawi[c] and Bassam Alameddine (iD) *[a,b]

A design strategy is disclosed to synthesize conjugated microporous polymers (CMPs) using a versatile copper-catalyzed [4 + 2] cyclobenzannulation reaction, which employs a diphenylethynyl terephthalaldehyde derivative **3** with a series of triptycene-based diethynyl aryl building blocks **2a–e**. Investigation of the intrinsic microporosity properties of **CBP1–5** using nitrogen adsorption measurements reveals Brunauer–Emmett–Teller (BET) surface areas up to 794 $m^2 g^{-1}$ and average pore volumes reaching 0.63 $cm^3 g^{-1}$. Inspection of the adsorption properties of the graphitic-like polymers **CBP1–5** divulges their high iodine uptake with a maximum of 166 wt%. Moreover, the target polymers **CBP1–5** prove their efficiency as selective dye adsorbents by removing up to 100% methylene blue over methyl orange from aqueous solution.

Introduction

Since the first report on the synthesis of conjugated microporous polymer (CMP) networks by Cooper *et al.*,[1] numerous scientists have contributed to that field, leading to a steep growth in the number of publications. Conjugated microporous polymers have emerged as promising materials for a wide range of cutting-edge fields,[2] mainly those related to sustainable energy applications, such as gas separation and storage,[3–6] hydrogen evolution,[7–9] organic solar cells (OSCs),[10–12] batteries,[13–16] field-effect transistors (FETs),[17–21] thermoelectrics,[22] sensors,[23,24] optical switches,[25–29] and light-emitting diodes (LEDs).[30–33] The eminence of CMPs stems from the exceptional properties that they exhibit, among others, their versatile synthesis, extended π-conjugation skeleton, high stability, and large surface area.[2] The chief advantage of CMP networks lies in their design that could be realized *via* numerous synthetic methodologies,[2] which span from transition-metal catalyzed cross-coupling reactions like Suzuki–Miyaura,[8,34–36] Sonogashira,[37–40] Yamamoto,[41–43] and

direct arylation[44,45] to several other synthetic approaches like oxidative coupling, condensation reactions, and cyclotrimerization, in addition to many other design strategies.[46–52]

Since the industrial revolution, fossil fuels have been increasingly utilized as the main feedstock in most human activities and technologies – reaching 85% of the total energy consumption in 2018 – which led to global economic developments and drastic improvements in our living standards.[53] Nevertheless, the combustion of fossil fuels instigates serious impacts on the environment caused by the generation of particulate matters (PMs) and massive release of various gases into the atmosphere, among others, carbon dioxide which contributes to global warming, acid rain and smog formation.[54] As the world demand for energy sources is on a sharp rise with an estimated energy consumption of 800 quadrillion British thermal units (BTUs) by 2040,[55] the development of sustainable energy sources with high efficiency and low-emission deems essential.[56] Amongst the alternative sources to fossil fuels, nuclear fission is considered a promising feedstock whose high efficiency in power generation is considered a major advantage, yet the formation of several radioactive gaseous byproducts, such as ^{85}Kr, ^{3}H, $^{14}CO_2$, ^{123}I, ^{125}I, and $^{127-140}I$, is believed to be a major drawback. In addition to the hitherto mentioned radioactive species, fission nuclear energy generates hydrogen- and alkyl-radioactive halides which are also considered hazardous due to their interference in metabolic processes.[57,58] As a result of the crucial need to develop highly efficient and cost-effective porous materials to capture

[a]Department of Mathematics and Natural Sciences, Gulf University for Science and Technology, Kuwait. E-mail: alameddine.b@gust.edu.kw; Tel: +965 2530 7476
[b]Functional Materials Group – CAMB, GUST, Kuwait
[c]Department of Chemistry, University of Kuwait, Kuwait

radioactive iodine-containing species, several adsorbents have been developed, namely, organic cages, silica gel, zeolites, and covalent-organic and metal–organic frameworks.[37,59–62]

On the other hand, several industrial processes discharge water-soluble non-biodegradable biologically active dyes, which could be either cationic, like methylene blue (MB), or anionic, such as methyl orange (MO) dyes. Some of these organic dyes are highly toxic, mutagenic, and carcinogenic.[63] In addition to their hazardous properties, the aforementioned pollutants cause several skin- and eye-related diseases, as well as various respiratory complications, which necessitates their removal from freshwater resources *via* sustainable techniques.[63–65] Various methods have been reported in the literature to remove organic dyes from water, of which we note photocatalytic degradation by employing H_2O_2[66] and $NaBH_4$,[67] electrodialysis,[68] membrane-based technology,[69] and the use of adsorbents, where the latter technique proved to be among the most prominent owing to its high efficiency, cost-effectiveness, simplicity, and possibility of being utilized under ambient conditions.[70,71]

We disclose the synthesis of five conjugated microporous polymers **CBP1–5** through a copper-catalyzed [4 + 2] benzannulation[72–74] from the reaction of various 1,4-diarylethynyl triptycene synthons **2a–e** with 2,5-bis(phenylethynyl) terephthalaldehyde **3**. The target polymers **CBP1–5** were obtained in excellent yields, and their intrinsic surface areas were thoroughly investigated before carrying out studies of their iodine uptake and organic dye adsorption.

Experimental section

Materials

All the reactions were carried out under an inert atmosphere using dry argon. All chemical reagents were used without further purification as purchased from Aldrich, Merck, and HiMedia unless otherwise specified. The comonomers **2a**, **2c**, **2e** and **3** were synthesized following the reported procedures in the literature.[59,73,75–78] Anhydrous solvents, namely, hexane, DCM, THF, DCE, TEA, methanol, diethyl ether, and acetone, were further dried over molecular sieves and deoxygenated by bubbling with argon gas for 30 minutes. Thin-layer chromatography (TLC) was performed on aluminum sheets coated with silica gel 60 F254 and revealed using a UV lamp. NMR (^{1}H: 600 MHz, ^{13}C: 150 MHz) spectra were recorded using a Bruker BioSpin GmbH 600 MHz spectrometer using CD_2Cl_2 as a solvent with the chemical shifts (δ) given in ppm and referenced to tetramethylsilane (TMS). Electron impact high-resolution mass spectra (EI-HRMS) were recorded on a Thermo Scientific DFS system with a standard PFK (perfluorokerosene) as a lock mass. The analysed data are converted to accurate mass employing the Xcalibur accurate mass calculation software. UV-Vis spectra were recorded using a Shimadzu UV1800 spectrophotometer. Photoluminescence (PL) spectra were recorded on an Agilent G9800 Cary Eclipse Fluorescence spectrophotometer. An Agilent Gel Permeation

Chromatograph (GPC/SEC) equipped with two columns (PL mixed-C) and calibrated against twelve monodisperse polystyrene (PS) standards, using THF as an eluent at a flow rate of 1.0 mL min^{-1}, was employed to determine the relative weight-average (M_w) and number-average (M_n) molecular weights and polydispersity indices ($Đ = M_w/M_n$) of all the reported polymers. FT-IR spectra were recorded on an FT/IR-6300 type A instrument using a KBr matrix. Single-crystal data collection was done on a Rigaku R-AXIS RAPID II diffractometer using filtered Mo-Kα radiation. The structure was solved by direct methods using the CrystalStructure crystallographic software package except for refinement, which was performed using SHELXL-97. The non-hydrogen atoms were refined anisotropically. Hydrogen atoms were refined using the riding model. Brunauer–Emmett–Teller (BET) surface area and porosity measurements were evaluated using a surface area and pore size analyzer (Gemini-V, Micromeritics, USA) at the boiling point of liquid nitrogen (−196 °C). Samples were deoxygenated in a VacuPrep 061 sample degassing system at a temperature of 120 °C overnight, before the experiments. Surface areas were calculated using the Brunauer–Emmett–Teller (BET) model of isotherms, and the adsorption of N_2 at small relative pressures. The total pore volume (V_t) was determined from the specific adsorption of N_2 at $p/p^0 = 0.99$. The t-plot method was used to estimate the micropore volume (V_{mic}) and external surface area (S_{ext}).

Synthesis

Synthesis of 2-((4-(*tert*-butyl)phenyl)ethynyl)benzaldehyde 1. A Schlenk tube was charged under argon with 2-bromobenzaldehyde (0.608 mL, 5.2 mmol, 1 eq.), 4-(*tert*-butyl)phenylacetylene (1.4 mL, 7.8 mmol, 1.5 eq.), $Pd_2(dba)_3$ (28 mg, 0.03 mmol, 6 mol%), and CuI (20 mg, 0.1 mmol) in 3 mL of deoxygenated diisopropylamine (iPr_2NH, 35 mmol) and the solution was refluxed overnight. The reaction mixture was then cooled to room temperature. After removal of the solvent under reduced pressure, the resulting mixture was dissolved in DCM and extracted with a saturated solution of $NaHCO_3$ (50 mL × 3). The combined organic layer was washed with deionized water (100 mL × 4), and the desired product was isolated using silica gel column chromatography with DCM/hexane (15 : 85 v/v) as the eluent yielding a pale yellow solid (1.25 g, 92%). ^{1}H-NMR (600 MHz, CD_2Cl_2, ppm): δ 10.68 (s, 1H, −*CHO*), 7.96 (d, 1H, J = 7.8 Hz ArH), 7.70 (d, 1H, J = 8.4, ArH) 7.63 (t, 1H, J = 7.7 Hz, ArH) 7.57 (d, 2H, J = 8.7 Hz ArH), 7.51–7.46 (m, 3H, ArH), 1.37 (s, 9H, −CH_3). ^{13}C-NMR (150 MHz, CD_2Cl_2, ppm): δ 192.09, 153.24, 136.45, 134.34, 133.75, 131.96, 129.06, 127.65, 127.52, 126.18, 119.85, 96.97, 84.88, 35.37, 31.44. FTIR (KBr, cm^{-1}): 2966, 2218, 1697. EI-HRMS: m/z calculated for M$^{•+1}$ $C_{19}H_{19}O$: 263.1436, found: 263.1436.

Synthesis of CBM1 (procedure A). A Schlenk tube was charged under argon with 2-((4-(*tert*-butyl)phenyl)ethynyl) benzaldehyde **1** (50 mg, 0.22 mmol, 2.2 eq.), 1,4-diethynyl triptycene **2a** (30 mg, 0.1 mmol, 1 eq.), copper(II) triflate Cu(OTf)$_2$ (7 mg, 0.02 mmol, 0.2 eq.), and trifluoroacetic acid TFA (30 μL, 0.4 mmol) in 5 mL of deoxygenated dichloroethane. The solu-

tion was heated at 100 °C overnight and the solvent was evaporated under reduced pressure. The resulting mixture was dissolved in DCM and extracted with a saturated solution of NaHCO$_3$ (50 mL × 2). The combined organic layer was washed with deionized water (100 mL × 3), concentrated, and the desired product was isolated using silica gel column chromatography with DCM/hexane (20 : 80 v/v) as the eluent. White solid (48 mg, 96%). ^{1}H-NMR (600 MHz, CD$_2$Cl$_2$, ppm): δ 8.13 (d, 2H, J = 8.4 Hz, ArH), 8.05 (d, 4H, J = 9.3 Hz, ArH), 8.00 (s, 2H, ArH) 7.69 (dd, 2H, J = 8.1 Hz, 1.6 Hz, ArH), 7.65 (m, 4H, ArH), 7.39 (q, 4H, J = 5.4 Hz, 2.2 Hz, ArH), 7.26 (s, 2H, ArH), 7.09 (q, 4H, J = 5.4 Hz, 2.4 Hz, ArH), 5.92 (s, 2H, triptycene-CH_s). ^{13}C-NMR (150 MHz, CD$_2$Cl$_2$, ppm): δ 146.06, 143.92, 138.44, 137.60, 134.12, 133.17, 128.86, 128.71, 128.65, 128.37, 128.32, 127.03, 126.98, 126.77, 126.21, 126.14, 125.95, 124.28, 51.52. EI-HRMS: m/z calculated for M$^{•+}$ C$_{40}$H$_{26}$: 506.2029, found: 506.2029.

Synthesis of CBM2. CBM2 was prepared following procedure A with 2-((4-(*tert*-butyl)phenyl)ethynyl)benzaldehyde **1** (65 mg, 0.25 mmol, 2.2 eq.), **2c** (65 mg, 0.11 mmol, 1 eq.), Cu(OTf)$_2$ (8 mg, 0.02 mmol, 0.2 eq.), and TFA (35 μL, 0.45 mmol) in 5 mL of deoxygenated dichloroethane. Pale yellow solid (83 mg, 94%). ^{1}H-NMR (600 MHz, CD$_2$Cl$_2$, ppm): δ 8.14 (s, 2H, ArH), 8.07 (t, 4H, J = 8.4 Hz, ArH), 7.95 (d, 2H, J = 7.4 Hz, ArH), 7.79 (d, 2H, J = 8.2 Hz, ArH), 7.63–7.61 (m, 6H, ArH), 7.25–7.22 (m, 8H, ArH), 7.13 (s, 4H, ArH), 5.59 (s, 2H, triptycene-CH_s), 1.32 (s, 9H, –$CH_{3,s}$), 1.25 (s, 9H, –$CH_{3,s}$). ^{13}C-NMR (150 MHz, CD$_2$Cl$_2$, ppm): δ 149.77, 146.17, 145.52, 143.96, 143.26, 139.56, 138.97, 137.59, 136.25, 135.94, 132.26, 130.75, 129.47, 127.56, 126.88, 126.22, 124.87, 124.77, 123.90, 123.38, 51.08, 34.27, 31.16. EI-HRMS: m/z calculated for M$^{•+}$ C$_{60}$H$_{50}$: 770.3913, found: 770.3913.

Synthesis of comonomer 2d. A Schlenk tube was charged under argon with 1,4-diethynyl triptycene **2a** (205 mg, 0.68 mmol, 1 eq.), 9-bromoanthracene (350 mg, 1.36 mmol, 2.0 eq.), bis(triphenylphosphine)palladium(II) dichloride PdCl$_2$(PPh$_3$)$_2$ (23 mg, 0.034 mmol), CuI (6.4 mg, 0.034 mmol), triethylamine (284 μL, 2.0 mmol), and 15 mL of deoxygenated THF and the reaction mixture was refluxed for 16 h. The solvent was evaporated under reduced pressure and the resulting mixture was extracted with dichloromethane from a saturated aqueous solution of NaHCO$_3$ (100 mL). The organic phase was washed with H$_2$O (100 mL × 3). The desired product was isolated by silica gel column chromatography, with DCM/hexane (30 : 70 v/v) as the eluent. Yellow solid (410 mg, 93%). ^{1}H NMR (600 MHz, CD$_2$Cl$_2$, ppm): δ 8.90 (d, J = 8.7 Hz, 4H, ArH), 8.62 (s, 2H, ArH) 8.17 (d, J = 8.5 Hz, 4H, ArH), 7.82–7.79 (m, 4H, ArH), 7.68–7.65 (m, 4H, ArH) 7.64 (q, J = 5.4, 3.2 Hz, 4H, ArH), 7.58 (s, 2H, ArH), 7.16 (q, J = 5.5, 3.1 Hz, 4H, ArH), 6.41 (s, 2H, triptycene–CH). ^{13}C NMR (150 MHz, CD$_2$Cl$_2$, ppm): δ 147.36, 144.66, 132.75, 131.32, 128.92, 128.29, 127.061, 126.58, 125.90, 125.68, 124.07, 119.01, 116.98, 98.32, 91.14, 52.56; EI-HRMS: m/z calculated for M$^{•+}$ C$_{52}$H$_{30}$: 654.2342, found: 654.2342.

Synthesis of polymer CBP1 (procedure B). 1,4-Diethynyl triptycene **2a** (145 mg, 0.48 mmol, 1 eq.), 2,5-bis(phenylethynyl)

terephthalaldehyde **3** (160 mg, 0.48 mmol, 1 eq.), Cu(OTf)$_2$ (70 mg, 0.192 mmol, 0.4 eq.), and TFA (295 μL, 3.84 mmol) were refluxed in 19 mL of deoxygenated dichloroethane in a Schlenk tube under argon. After 2 days of reaction, the precipitate was filtered and washed exhaustively with a sequence of solvents (50 mL of DCM, 50 mL of THF, 50 mL of MeOH, 50 mL of water, and 50 mL of diethyl ether) affording a deep red solid (200 mg, 98%). ^{1}H NMR (600 MHz, CD$_2$Cl$_2$, ppm): δ 8.78 (br, 2H, ArH), 8.38 (br, 2H, ArH) 7.8–6.8 (m, 14H, ArH), 5.9 (br-d, 2H, triptycene–CH). ^{13}C NMR (150 MHz, CD$_2$Cl$_2$, ppm): δ 145.82, 145.73, 129.09, 129.02, 127.06, 126.72, 126.28, 126.06, 125.03, 124.17, 51.68; FTIR (KBr, cm^{-1}): 2960 (Ar–CH str.), 1680 (Ar–CH ben.), 1423 (Ar–C═C ben.); UV-vis: (THF, 10^{-8} M), λ_{max} [nm] = 298, fluorescence: (THF, 10^{-8} M), λ_{max} [nm] = 458.

Synthesis of CBP2. CBP2 was prepared following procedure B with 2,5-bis(phenylethynyl)terephthalaldehyde **3** (166 mg, 0.5 mmol, 1 eq.), **2b** (226 mg, 0.5 mmol, 1 eq.), Cu(OTf)$_2$ (72 mg, 0.2 mmol, 0.4 eq.), and TFA (308 μL, 2.0 mmol) in 20 mL of deoxygenated dichloroethane. Deep red solid (275 mg, 96%). FTIR (KBr, cm^{-1}): 3030 (Ar–CH str.), 1705 (Ar–CH ben.), 1456 (Ar–C═C ben.); UV-vis: (THF, 10^{-8} M), λ_{max} [nm] = 298, fluorescence: (THF, 10^{-8} M), λ_{max} [nm] = 343, 370, 400.

Synthesis of CBP3. CBP3 was prepared following procedure B with 2,5-bis(phenylethynyl)terephthalaldehyde **3** (234 mg, 0.7 mmol, 1 eq.), **2c** (396 mg, 0.7 mmol, 1 eq.), Cu(OTf)$_2$ (101 mg, 0.28 mmol, 0.4 eq.), and TFA (431 μL, 5.6 mmol) in 28 mL of deoxygenated dichloroethane. Deep red solid (450 mg, 93%). GPC (THF); M_w (g mol^{-1}): 30 187 M_n (g mol^{-1}): 60 288, Đ: 2.00; FTIR (KBr, cm^{-1}): 3023 (Ar–CH), 2964 (aliphatic–CH str.), 1699 (Ar–CH ben.), 1460 (Ar–C═C ben.); UV-vis: (THF, 10^{-8} M), λ_{max} [nm] = 315, fluorescence: (THF, 10^{-8} M), λ_{max} [nm] = 478.

Synthesis of CBP4. CBP4 was prepared following procedure B with 2,5-bis(phenylethynyl)terephthalaldehyde **3** (100 mg, 0.3 mmol, 1 eq.), **2d** (196 mg, 0.3 mmol, 1 eq.), Cu(OTf)$_2$ (43 mg, 0.12 mmol, 0.4 eq.), and TFA (184 μL, 2.4 mmol) in 12 mL of deoxygenated dichloroethane. Deep red solid (225 mg, 96%). FTIR (KBr, cm^{-1}): 3030 (Ar–CH str.), 1667 (Ar–CH ben.), 1460 (Ar–C═C ben.); UV-vis: (THF, 10^{-8} M), λ_{max} [nm] = 298, fluorescence: (THF, 10^{-8} M), λ_{max} [nm] = 404, 430, 455.

Synthesis of CBP5. CBP5 was prepared following procedure B with 2,5-bis(phenylethynyl)terephthalaldehyde **3** (90 mg, 0.27 mmol, 1 eq.), **2e** (190 mg, 0.27 mmol, 1 eq.), Cu(OTf)$_2$ (39 mg, 0.10 mmol, 0.4 eq.), and TFA (166 μL, 2.1 mmol) in 11 mL of deoxygenated dichloroethane. Deep red solid (218 mg, 97%). FTIR (KBr, cm^{-1}): 3026 (Ar–CH str.), 1681 (Ar–CH ben.), 1463 (Ar–C═C ben.); UV-vis: (THF, 10^{-8} M), λ_{max} [nm] = 298, fluorescence: (THF, 10^{-8} M), λ_{max} [nm] = 403, 429, 456.

Dye adsorption studies of CBP1–5

5 mg of **CBP1–5** were immersed in a 5 mL aqueous solution of a dye (MB or MO) and the solution was stirred at room temperature. The UV-visible spectra of the solutions were then recorded after specific time intervals.

Results and discussion

Synthesis of prototypical monomers

As a proof of concept, the prototypical monomer **CBM1** was prepared in 92% yield using a copper-catalyzed [4 + 2] cyclo-benzannulation reaction from 1,4-diethynyltriptycene **2a**[76] with two equivalents of 2-((4-(*tert*-butyl)phenyl)ethynyl)benz-aldehyde **1** in refluxing dichloroethane (Scheme 1). The structure of **CBM1** was confirmed by ^{1}H- and ^{13}C-nuclear magnetic resonance (NMR), high-resolution mass spectroscopy (HRMS), and single crystal X-ray diffraction (XRD) (see Fig. 1 and 2 and related figures in the ESI†).

Fig. 1 portrays the comparative ^{1}H-NMR spectra of synthons **1**, **2a** and **CBM1** where the spectrum of the latter prototypical monomer clearly confirms the presence of the desired peaks and the disappearance of all peaks related to the starting materials **1** and **2a**, namely, the fingerprint chemical shifts of the carbaldehyde group at 10.66 ppm and the *t*-butyl group at 1.37 ppm for synthon **1** in addition to the proton peak of the ethynyl group of **2a** at 3.47 ppm. The chemical shifts ranging from 7.0 ppm to 8.1 ppm are attributed to the aromatic protons of **CBM1** while the peak detected at 5.9 ppm portrays the characteristic tertiary triptycene hydrogens (*cf.* peaks labeled **e** in Fig. 1). The distinctive peaks of the starting materials completely disappear in the ^{1}H-NMR spectrum of **CBM1**, namely that of the terminal hydrogen of the ethynyl groups detected at 3.6 ppm in **2a**[79] in addition to the proton peaks of the aldehyde and *t*-butyl groups in synthon **1** detected at 10.6 ppm and 1.3 ppm, respectively (see Fig. S1 and S2 in the ESI†). On the other hand, the ^{13}C-NMR spectrum of **CBM1** displays all the expected aromatic peaks in the range of 146.0–124.2 ppm in addition to the chemical shift of the sp^3 carbon of the triptycene unit at 51.52 ppm (see Fig. S7 in the ESI†). Furthermore, the high purity of **CBM1** was confirmed by electron-impact high-resolution mass spectrometry (EI-HRMS, see Fig. S12 in the ESI†). Similarly, the replacement of the terminal sp-hybridized hydrogen atoms in **2a** by the more sterically demanding *p-tert*-butylphenyl group (*i.e.* **2c**) resulted

in the formation of the prototypical monomer **CBM2** in 94% yield (Scheme 1). The structure of the latter compound was confirmed by ^{1}H- and ^{13}C-NMR as well as EI-HRMS (see Fig. 2 and related figures in the ESI†).

Single crystals of **CBM1–2** were grown by depositing a layer of hexane on top of a solution of the monomers in dichloro-methane. The molecular structures of **CBM1–2** were investigated by single crystal X-ray diffraction, thus confirming the deviation of the pending naphthyl rings from planarity and leading, consequently, to highly branched structures in space (Fig. 2).

Synthesis of polymers CBP1–5

Synthesis of the target conjugated polymers **CBP1–5** (Scheme 2) was carried out using reaction conditions similar to those employed to make the prototypical monomers **CBM1–2** described in Scheme 1. The copper-catalyzed [4 + 2] cyclobenzannulation reaction of various 1,4-diethynyl tripty-cene derivatives **2a–e** (with R = H, aryl) and 2,5-bis(phenylethy-nyl)terephthalaldehyde **3** afforded the target conjugated poly-mers **CBP1–5** in excellent yields (Scheme 2). These latter poly-mers were decorated with various side groups like simple hydrogen atoms (**CBP1**), phenyl (**CBP2**) and *p-tert*-butylphenyl (**CBP3**) groups, as well as with the more sterically hindered anthracene (**CBP4**) and pyrene (**CBP5**) moieties.

It is worthwhile to note that the degree of polymerization (DP) of the target conjugated polymers **CBP1–5** was improved by optimizing both the reactants' concentration and reaction time (Table 1). Therefore, the polymerization reaction of a 0.01 M solution of **2a** with an equimolar amount of **3** in the presence of copper(II) triflate Cu(OTf)$_2$ and trifluoroacetic acid (TFA) in refluxing dichloroethane (DCE) for 24 hours afforded **CBP1** in 58% yield. Gel permeation chromatography (GPC) analysis of the latter target polymer revealed a number average molecular weight M_n of ≈5.5 kDa and polydispersity index $Đ = M_w/M_n$ of ~4.0 (Table 1, entry 1). When the reaction time was prolonged to 48 h, the M_n value slightly increased to ~7.4 kDa whereas the polydispersity index $Đ$ decreased to ~3.8 (Table 1,
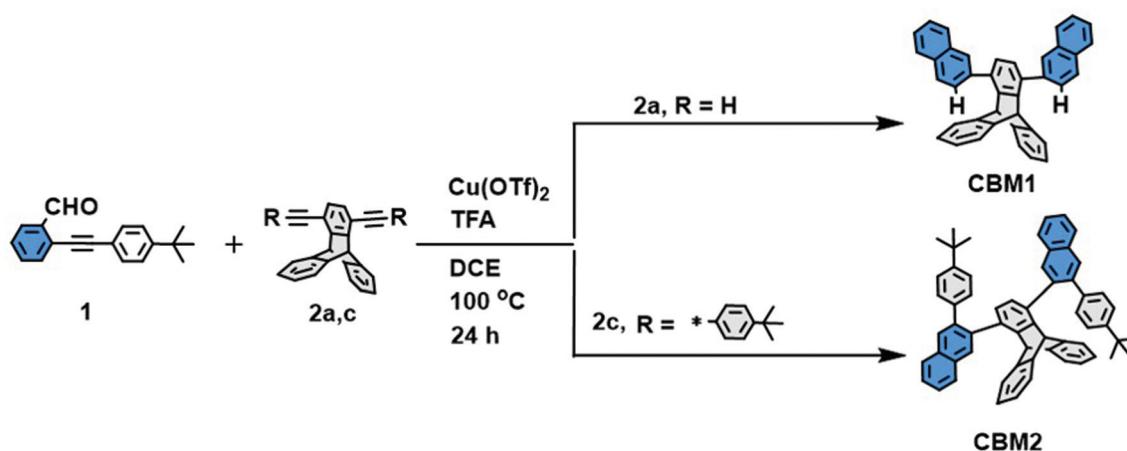
Scheme 1 Synthesis of prototypical monomers **CBM1–2**.
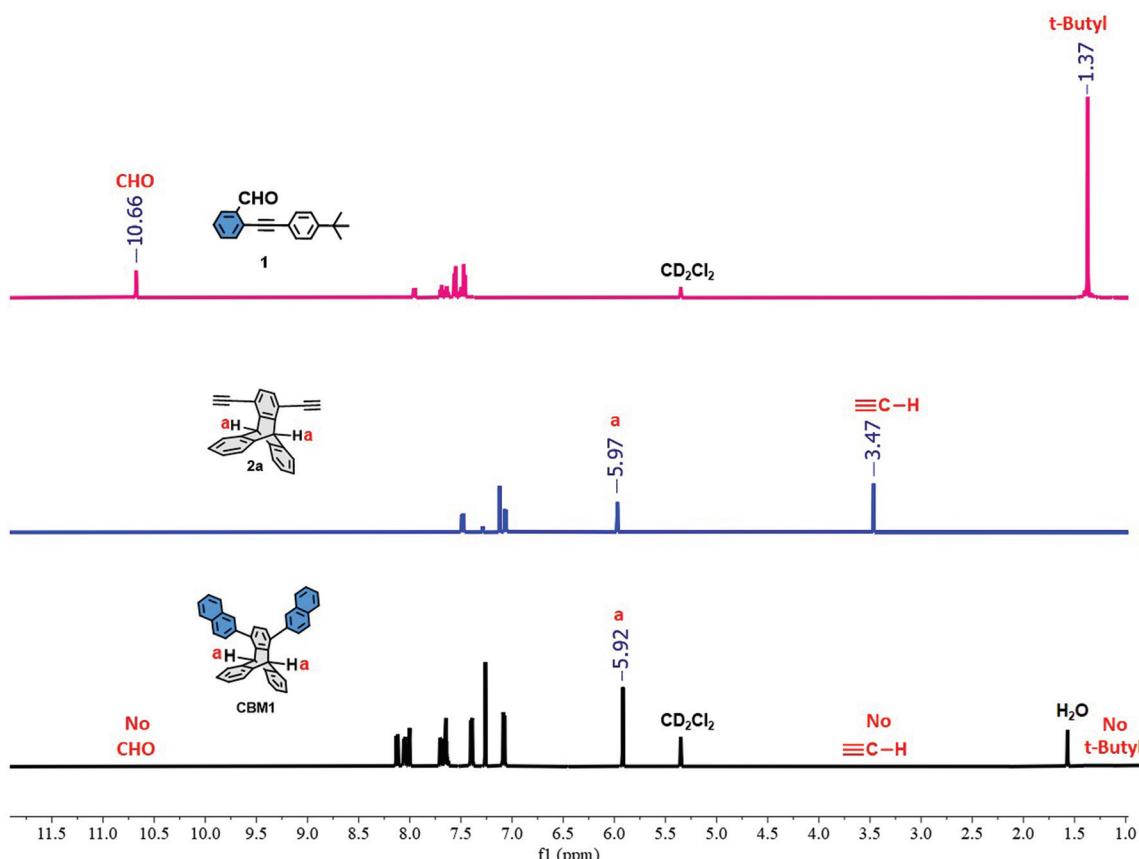
Fig. 1 Comparative ^{1}H-NMR of **1**, **2a**, and **CBM1**.
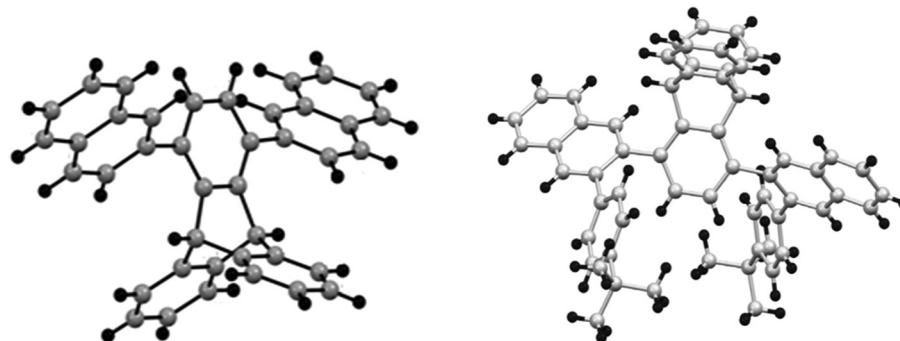
Fig. 2 Single crystal structures of **CBM1** (left) and **CBM2** (right).
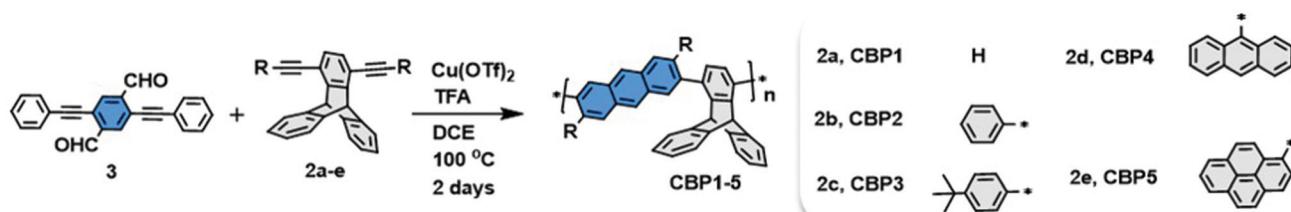
Scheme 2 Synthesis of polymers **CBP1–5**.

Table 1 Optimization conditions of the cyclobenzannulation polymerization reaction

Entry	Polymer[a]	Time (h)	Yield (%)	$C_M{}^{b}$ [M]	M_n (KDa)	M_w (KDa)	$Đ$
1	**CBP1**	24	58	1.0	5.5	22	4.0
2	**CBP1**	48	79	1.0	7.4	28	3.8
3	**CBP1**	96	75	1.0	7.0	41	5.8
4	**CBP1**	48	100	2.5	Insoluble	—	—
5	**CBP2**	48	87	2.5	Insoluble	—	—
6	**CBP3**	48	100	2.5	30	60	2.0
7	**CBP4**	48	85	2.5	Insoluble	—	—
8	**CBP5**	48	100	2.5	Insoluble	—	—

[a] Cu(OTf)$_2$(0.4 eq.), TFA (8.0 eq.), and DCE. [b] Molar concentration ×10^{-2} of **3**.

entry 2). A further increase of the reaction time to 96 h did not improve the number average molecular weight M_n whose value stagnated at ~7.0 kDa but recorded a very high polydispersity index $Đ$ of 5.7 (Table 1, entry 3). It is noteworthy that the formation of **CBP1** was further confirmed by ^{1}H- and ^{13}C-NMR spectroscopy (see Fig. S5 and S10 in the ESI†). However, the increasing polydispersity index that is accompanied by a relatively low number average molecular weight M_n, which does not improve even when prolonging the reaction time, could be explained by the low concentration of the reactants, thus leading to a non-homogeneous distribution of the polymers chains in solution during the reaction. Therefore, increasing the molar concentrations of monomers **2a** and **3** to 0.025 M and maintaining the reaction for 48 h afforded polymer **CBP1** as an insoluble brown powder in quantitative yield (Table 1, entry 4). The improvement of the degree of polymerization of the cyclobenzannulation reactions was further confirmed by preparing the target polymer **CBP3** which contains *tert*-butyl side groups allowing for its GPC analysis that revealed a number average molecular weight M_n of ≈30 kDa with a polydispersity index $Đ$ of ~2.0. After optimization of the reaction

conditions, the conjugated polymers **CBP1–5** were all obtained in excellent yields but were found to be insoluble in common organic solvents, which limited their characterization to FTIR, UV-vis absorption and emission spectroscopies (see Fig. 3 and 4 and related figures in the ESI†).

Fig. 3 shows the comparative FT-IR absorption spectra of comonomers **3** and **2a** besides their corresponding target polymer **CBP1**. The characteristic stretching vibrations of the alkynyl (C≡C) and carbonyl (C=O) groups in **3** are observed at 2136 cm^{-1} and 1644 cm^{-1}, respectively. Similarly, the characteristic stretching vibrations of the terminal alkyne (≡C–H) and alkynyl (C≡C) in **2a** can be detected at 3276 cm^{-1} and 2105 cm^{-1}. All the stretching vibrations for the distinctive functional groups of synthons **2a** and **3** (*i.e* ≡C–H, C≡C and C=O) completely disappeared in the FT-IR absorption spectrum of the target conjugated polymer **CBP1**, thereby proving the complete cyclobenzannulation reaction. It is noteworthy that the FT-IR spectrum of **CBP1** discloses more pronounced aromatic C=C and C–H bending and stretching vibrations in the regions of 1600–1400 cm^{-1} and 3050–2960 cm^{-1}, respectively, when compared to the corresponding stretching
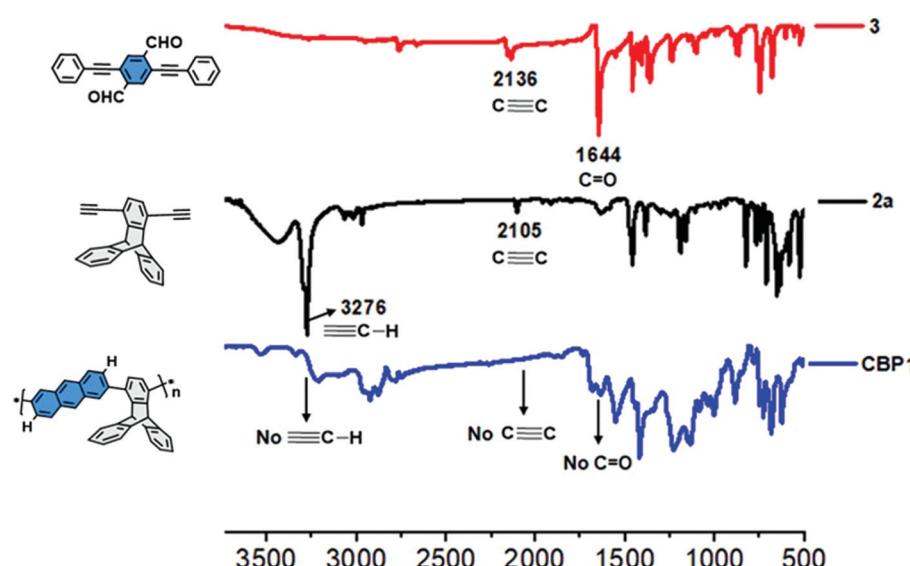

Fig. 3 Comparative FT-IR spectra of **3** (red), **2a** (black), and **CBP1** (blue).
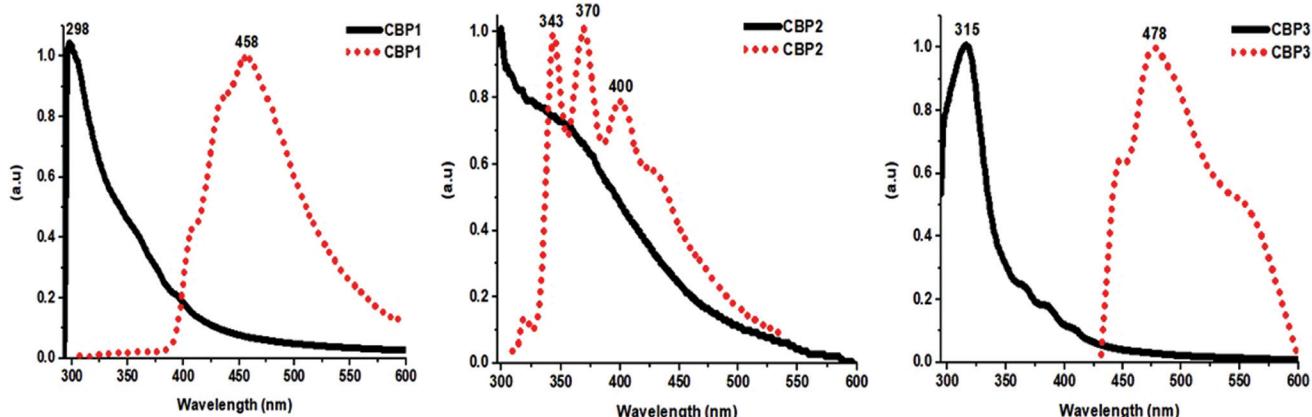
Fig. 4 Normalized UV-VIS absorption (solid lines) and emission (dotted lines) spectra of **CBP1–3** ($C_M = 10^{-8}$ M in THF).

vibrations recorded for the starting materials **2a** and **3**. This further confirms the full conversion of the aldehyde and ethynyl moieties into the corresponding aryl groups.

The photophysical properties of the target polymers were measured by means of UV-Vis absorption and fluorescence spectroscopies (see Fig. 4 and Fig. S18 in the ESI†). **CBP1, 2, 4** and **5** display similar features with a strong UV absorption band at 298 nm whereas **CBP3**, *i.e.* the polymer that contains tertiary butyl groups, discloses a strong absorption band at 315 nm, thus revealing a red shift by 17 nm (Fig. 4). The emission spectrum of **CBP1** portrays a broad peak whose maximum is detected at ~458 nm, where the latter could be attributed to the fingerprint region of the newly formed anthracene units (Fig. 4). On the other hand, while the emission spectrum of **CBP2** displays three distinctive peaks at 343 nm, 370 nm, and 400 nm, the fluorescence of **CBP3** discloses a broader red-shifted peak with an emission maximum at 478 nm. Interestingly, both target polymers **CBP4** and **CBP5** portray similar emission spectra with characteristic peaks at 404 nm, 430 nm, and 455 nm (see Fig. S18 in the ESI†).

BET surface area studies

Microporosity properties of **CBP1–5** were investigated by carrying out N_2 adsorption experiments at 77 K and a low relative pressure (Fig. 5). Table 2 shows the Brunauer–Emmett–Teller (BET) surface areas and pore volumes derived from these isotherms. The conjugated polymer **CBP1** shows a scarce BET surface area of ~3.0 m² g⁻¹ (Table 2, entry 1). Conjugated polymer **CBP2**, *i.e.* bearing phenyl side groups, shows a surface area of 143 m² g⁻¹ (Table 2, entry 2). The polymers bearing anthracene (**CBP4**) and pyrene (**CBP5**) side groups reveal

Table 2 Summary of BET results of polymers **CBP1–5**

Entry	Polymer	BET surface area (m² g⁻¹)	Pore volume (cm³ g⁻¹)
1	**CBP1**	3.0	0.005
2	**CBP2**	143	0.11
3	**CBP3**	794	0.63
4	**CBP4**	98	0.09
5	**CBP5**	203	0.16
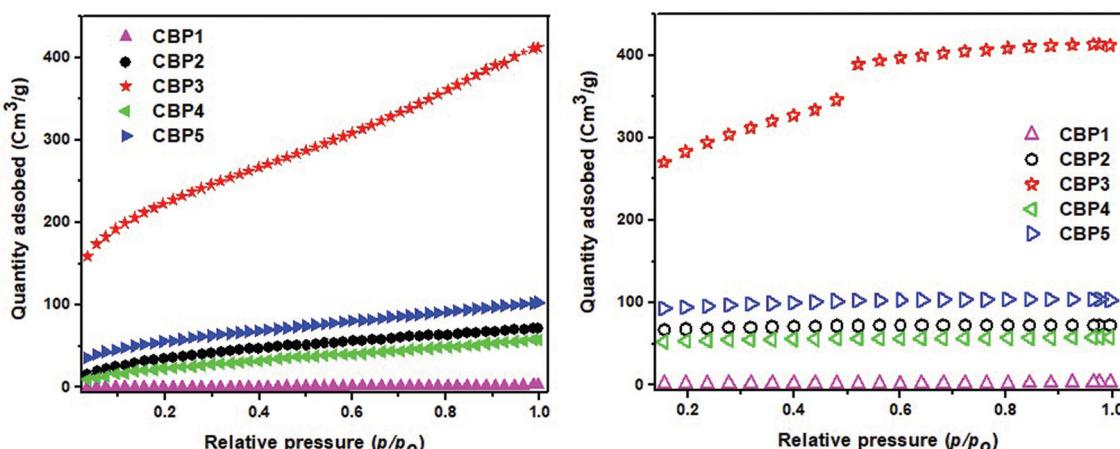
Fig. 5 Nitrogen adsorption (left) and desorption isotherms (right) of **CBP1–5** measured at 77 K.

surface areas of 98 m^2 g^{-1} and 203 m^2 g^{-1}, respectively (Table 2, entries 4 and 5). Interestingly, the conjugated polymer bearing the bulky *tert*-butylphenyl side groups, **CBP3**, displays the largest surface area of 794 m^2 g^{-1} (Table 2, entry 3). It is worthwhile to note the hysteresis of N$_2$ adsorption/desorption isotherms for **CBP3** with significant N$_2$ uptake at a low relative pressure (p/p^0), which is considered as the primary indicator of microporosity (Fig. 5).

Iodine adsorption studies

The graphitic-like structures of **CBP1–5** polymers and their porous properties with BET surface areas reaching up to 794 m^2 g^{-1} render them potential candidates as adsorbent materials, which have prompted us to explore their iodine uptake properties. Therefore, gravimetric analysis of iodine vapor adsorption[59,80] was carried out by taking a 20 mg sample from each of the polymers **CBP1–5** and exposing it to iodine vapors in an open glass vial, which was in turn placed inside a sealed glass vessel that contains excess iodine crystals heated at 80 °C under atmospheric pressure. The target polymers **CBP1–4** revealed iodine uptake values ranging between 101 wt% and 145 wt% after 24 hours of exposure to iodine vapors (Table 3). Interestingly, ∼102 wt% was adsorbed by **CBP5** after the first hour of exposure to iodine vapors, and which reached ∼166 wt% after 24 hours (Fig. 6). Furthermore, it has been noticed that the iodine adsorption values do not increase even when the target polymers **CBP1–5** were kept under excess vapors of iodine for 48 hours, which suggests the saturation of **CBP1–5** after 24 hours of exposure to iodine. The

record value of 166 wt% of iodine uptake by **CBP5** is considered to be promising when compared to the iodine adsorbent materials reported in the literature, namely, conjugated microporous polymers (200 wt%),[59] hierarchically porous adamantane-based macromolecules (202 wt%),[61] conjugated microporous polymers with thiophene units (222 wt%),[81] nitrogen-rich triptycene-based materials (180 wt%),[82] calix[4]arene-based 2D macromolecules (114 wt%),[83] porphyrin and pyrene-based conjugated microporous polymers (130 wt%),[84] JLUE covalent organic polymers (∼90 wt%),[57] triazine-based covalent frameworks (177 wt%),[47] and fluorine-enriched polymers (141 wt%).[37]

The complete desorption efficiency of the iodine-loaded polymers (I$_2$@**CBP1–5**) was recorded at different time intervals where the iodine vapors adsorbed by **CBP1–5** were released by simple heating of the latter polymers in the air at 120 °C (Fig. 6 and Table 3). The reusability of the polymers was also investigated using **CBP5** as a model candidate where a sample of **CBP5** fully loaded with iodine vapors (I$_2$@**CBP5**) was heated at 120 °C for 24 hours, in order to ensure the complete release of the adsorbate from the polymer backbone. The reactivated **CBP5** was then exposed to iodine vapors and its uptake was recorded gravimetrically using the procedure described above, revealing an uptake pattern similar to that of a freshly prepared polymer. The iodine adsorption–desorption cycles were repeated several times showing no change in iodine uptake, and thus, confirming the possibility of regenerating the polymers.

Dye adsorption studies

Dye adsorption tests were investigated by soaking a sample of the conjugated target polymers **CBP1–5** in various dyes' aqueous solutions, in particular, methyl orange (MO), an anionic pigment, and methylene blue (MB), a cationic dye (see Fig. 7 and Fig. S19–22 in the ESI†). The efficiency of MB and MO dye removal from water by polymers **CBP1–5** was investigated by recording the UV-visible absorbance spectra of the dyes' aqueous solutions at different time intervals. The dye adsorption experiments were carried out by stirring a 5 mg sample of polymers **CBP1–5** in a 5 mL aqueous solution of MB

Table 3 Summary of iodine adsorption and desorption of polymers **CPP1–5**

| Entry	Polymer	Wt% I$_2$ adsorption In 24 h	Wt% I$_2$ desorption In 180 min
1	**CBP1**	145	137
2	**CBP2**	101	101
3	**CBP3**	135	135
4	**CBP4**	140	132
5	**CBP5**	166	166
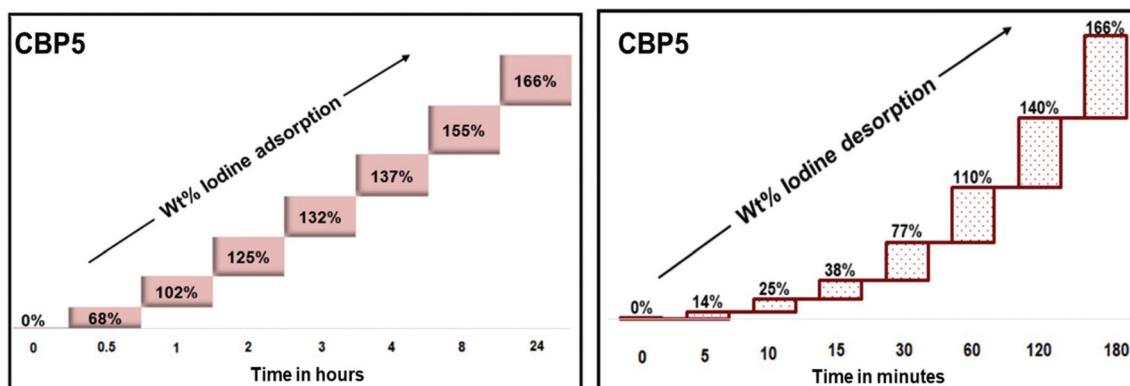
**Fig. 6** Wt% iodine adsorption (left) and desorption (right) graphs of **CBP5**.
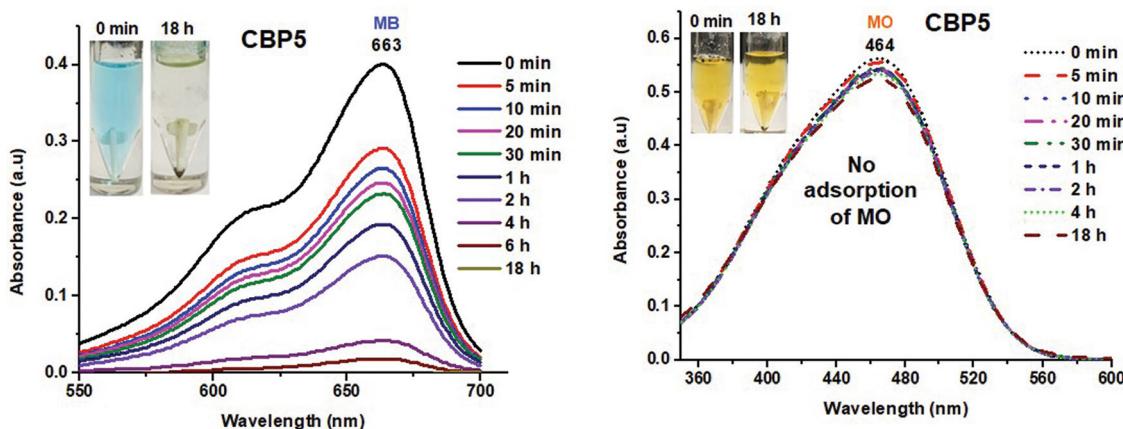
Fig. 7 MB (left) and MO (right) adsorption by **CBP5** at various time intervals (inset: photographs showing the color change upon dye adsorption).

(5 mg L^{-1}) at ambient temperature. A conspicuous decrease in the intensity of the MB absorbance maximum peak at 663 nm was observed, which confirms the adsorption of MB by polymers **CBP1–5**. Interestingly, more than 90% of MB dye was removed after stirring either **CBP2** or **CBP5** for 4 hours in the dye solution, which reached 100% MB adsorption when kept in solution overnight at room temperature. On the other hand, target polymers **CBP1**, **3** and **4** were found to adsorb up to ~60%, ~40%, and ~90%, respectively, of MB when they were kept in the aqueous solution overnight at room temperature (see Fig. S19–S22 in the ESI†). MB adsorption could be noticed physically where the color of the solution faded from blue to colorless (Fig. 7, inset), and which proves the efficient removal of this dye from water by polymers **CBP1–5**. In contrast to its high uptake of MB, target polymer **CBP5** was found to adsorb an insignificant amount of MO even after stirring it overnight at room temperature in the dye aqueous solution (Fig. 7).

Selective adsorption and separation of dyes is one of the ways to assess the performance of a material as an adsorbent

of a particular dye and/or a group of dyes. Therefore, the adsorption selectivity of polymer **CBP5** over cationic/anionic dyes was explored by stirring 5 mg of polymer **CBP5** at ambient temperature in a 5 ml aqueous solution of an equal mixture of the cationic MB (5 mg L^{-1}) and anionic MO (5 mg L^{-1}) dyes. The UV-visible spectra were recorded at different time intervals to investigate the adsorption of the two dyes present in solution (Fig. 8). Interestingly, the green solution mixture of MB and MO turned orange only after 5 minutes from the addition of **CBP5** (Fig. 8 inset) where the UV-Visible absorption spectroscopy disclosed that more than 80% of the cationic MB dye was removed as evidenced by a sharp decrease in the characteristic maximum absorption peak of MB at ~663 nm (Fig. 8). It is noteworthy that even when the solution is stirred overnight, only ~10% of MO was adsorbed by **CBP5**, which strongly suggests that **CBP5** can be employed as a selective sorbent material for cationic dyes such as MB over anionic dyes like MO.

Fig. 8 Selective dye removal capability of **CBP5** from a mixed solution of MB and MO (inset: photographs showing the color change after MB adsorption)

Conclusion

A novel synthetic methodology which consists of employing a copper-catalyzed [4 + 2] cyclobenzannulation polymerization reaction is disclosed leading to the formation of five conjugated graphitic-like polymers **CBP1–5** in excellent yields. The conjugated polymers reveal high BET surface areas reaching up to 794 m^2 g^{-1} and average pore volumes of 0.63 cm^3 g^{-1}. Iodine uptake tests of **CBP1–5** demonstrate adsorption rates in the range of ~101–166 wt%. Dye adsorption from aqueous solution using **CBP1–5** show excellent and selective dye adsorbent properties reaching up to 100% removal of the toxic methylene blue over methyl orange at ambient temperature. The modular synthetic strategy, in addition to the promising microporous properties, and the use of these polymers as iodine and cationic dye adsorbents qualify these polymers to be considered as prominent materials for environmental and energy applications.

Conflicts of interest

There are no conflicts to declare.

Acknowledgements

References

1 J.-X. Jiang, F. Su, A. Trewin, C. D. Wood, N. L. Campbell, H. Niu, C. Dickinson, A. Y. Ganin, M. J. Rosseinsky, Y. Z. Khimyak and A. I. Cooper, *Angew. Chem., Int. Ed.*, 2007, **46**, 8574–8578.

2 J.-S. M. Lee and A. I. Cooper, *Chem. Rev.*, 2020, **120**, 2171–2214.

3 H. Hong, Z. Guo, D. Yan and H. Zhan, *Microporous Mesoporous Mater.*, 2020, **294**, 109870.

4 D. Taylor, S. J. Dalgarno, Z. Xu and F. Vilela, *Chem. Soc. Rev.*, 2020, **49**, 3981–4042.

5 S.-J. Yang, X. Ding and B.-H. Han, *Macromolecules*, 2018, **51**, 947–953.

6 D. Reinhard, W.-S. Zhang, Y. Vaynzof, F. Rominger, R. R. Schröder and M. Mastalerz, *Chem. Mater.*, 2018, **30**, 2781–2790.

7 R. S. Sprick, Y. Bai, A. A. Y. Guilbert, M. Zbiri, C. M. Aitchison, L. Wilbraham, Y. Yan, D. J. Woods, M. A. Zwijnenburg and A. I. Cooper, *Chem. Mater.*, 2019, **31**, 305–313.

8 Y. Zhao, W. Ma, Y. Xu, C. Zhang, Q. Wang, T. Yang, X. Gao, F. Wang, C. Yan and J.-X. Jiang, *Macromolecules*, 2018, **51**, 9502–9508.

9 X. Wang, L. Chen, S. Y. Chong, M. A. Little, Y. Wu, W.-H. Zhu, R. Clowes, Y. Yan, M. A. Zwijnenburg, R. S. Sprick and A. I. Cooper, *Nat. Chem.*, 2018, **10**, 1180–1189.

10 J. Yang, P. Cong, L. Chen, X. Wang, J. Li, A. Tang, B. Zhang, Y. Geng and E. Zhou, *ACS Macro Lett.*, 2019, **8**, 743–748.

11 K. Aoshima, M. Nomura and A. Saeki, *ACS Omega*, 2019, **4**, 15645–15652.

12 H. Huang, H. Bin, Z. Peng, B. Qiu, C. Sun, A. Liebman-Pelaez, Z.-G. Zhang, C. Zhu, H. Ade, Z. Zhang and Y. Li, *Macromolecules*, 2018, **51**, 6028–6036.

13 S. Gu, S. Wu, L. Cao, M. Li, N. Qin, J. Zhu, Z. Wang, Y. Li, Z. Li, J. Chen and Z. Lu, *J. Am. Chem. Soc.*, 2019, **141**(24), 9623–9628.

14 S. Xu, G. Wang, B. P. Biswal, M. Addicoat, S. Paasch, W. Sheng, X. Zhuang, E. Brunner, T. Heine, R. Berger and X. Feng, *Angew. Chem., Int. Ed.*, 2018, **58**, 849–853.

15 C.-F. Yao, K.-L. Wang, H.-K. Huang, Y.-J. Lin, Y.-Y. Lee, C.-W. Yu, C.-J. Tsai and M. Horie, *Macromolecules*, 2017, **50**, 6924–6934.

16 H. Wang, Z. Cheng, Y. Liao, J. Li, J. Weber, A. Thomas and C. F. J. Faul, *Chem. Mater.*, 2017, **29**, 4885–4893.

17 V. Lakshmi, C.-H. Liu, M. Rajeswara Rao, Y. Chen, Y. Fang, A. Dadvand, E. Hamzehpoor, Y. Sakai-Otsuka, R. S. Stein and D. F. Perepichka, *J. Am. Chem. Soc.*, 2020, **142**, 2155–2160.

18 S.-H. Kang, A. Jeong, H. R. Lee, J. H. Oh and C. Yang, *Chem. Mater.*, 2019, **31**, 3831–3839.

19 Y. Du, H. Yao, L. Galuska, F. Ge, X. Wang, H. Lu, G. Zhang, X. Gu and L. Qiu, *Macromolecules*, 2019, **52**, 4765–4775.

20 F. Chen, Y. Jiang, Y. Sui, J. Zhang, H. Tian, Y. Han, Y. Deng, W. Hu and Y. Geng, *Macromolecules*, 2018, **51**, 8652–8661.

21 T. M. Swager, *Macromolecules*, 2017, **50**, 4867–4886.

22 X. Yan, M. Xiong, J.-T. Li, S. Zhang, Z. Ahmad, Y. Lu, Z.-Y. Wang, Z.-F. Yao, J.-Y. Wang, X. Gu and T. Lei, *J. Am. Chem. Soc.*, 2019, **141**, 20215–20221.

23 R. Sun, S. Feng, B. Zhou, Z. Chen, D. Wang and H. Liu, *ACS Macro Lett.*, 2020, **9**, 43–48.

24 A. Hirose, K. Tanaka, R. Yoshii and Y. Chujo, *Polym. Chem.*, 2015, **6**, 5590–5595.

25 T. Ikai, T. Yoshida, K.-I. Shinohara, T. Taniguchi, Y. Wada and T. M. Swager, *J. Am. Chem. Soc.*, 2019, **141**, 4696–4703.

26 B. Alameddine, N. Baig, S. Shetty and S. Al-Mousawi, *Polymer*, 2019, **178**, 121589.

27 N. Baig, S. Shetty, S. Al-Mousawi, F. Al-Sagheer and B. Alameddine, *Mater. Today Chem.*, 2018, **10**, 213–220.

28 K. Aravindu, E. Cloutet, C. Brochon, G. Hadziioannou, J. Vignolle, F. Robert, D. Taton and Y. Landais, *Macromolecules*, 2018, **51**, 5852–5862.

29 Z. Wang, C. Wang, Y. Fang, H. Yuan, Y. Quan and Y. Cheng, *Polym. Chem.*, 2018, **9**, 3205–3214.

30 B. Alameddine, S. Shetty, N. Baig and S. Al-Mousawi, *Mater. Today Chem.*, 2019, **14**, 100190.

31 A. Leventis, J. Royakkers, A. G. Rapidis, N. Goodeal, M. K. Corpinot, J. M. Frost, D.-K. Bučar, M. O. Blunt, F. Cacialli and H. Bronstein, *J. Am. Chem. Soc.*, 2018, **140**, 1622–1626.

32 A. Ichige, H. Saito, J. Kuwabara, T. Yasuda, J.-C. Choi and T. Kanbara, *Macromolecules*, 2018, **51**, 6782–6788.

33 M. J. Sung, S. Yoon, S.-K. Kwon, Y.-H. Kim and D. S. Chung, *ACS Appl. Mater. Interfaces*, 2016, **8**, 31172–31178.

34 S. Shetty, N. Baig, A. Hassan, S. Al-Mousawi, N. Das and B. Alameddine, *Microporous Mesoporous Mater.*, 2020, **303**, 110256.

35 J. M. Tobin, J. Liu, H. Hayes, M. Demleitner, D. Ellis, V. Arrighi, Z. Xu and F. Vilela, *Polym. Chem.*, 2016, **7**, 6662–6670.

36 K. Zhang, Z. Vobecka, K. Tauer, M. Antonietti and F. Vilela, *Chem. Commun.*, 2013, **49**, 11158–11160.

37 G. Li, C. Yao, J. Wang and Y. Xu, *Sci. Rep.*, 2017, **7**, 13972.

38 J. Choi, J. H. Ko, C. W. Kang, S. M. Lee, H. J. Kim, Y.-J. Ko, M. Yang and S. U. Son, *J. Mater. Chem. A*, 2018, **6**, 6233–6237.

39 B. C. Ma, S. Ghasimi, K. Landfester, F. Vilela and K. A. I. Zhang, *J. Mater. Chem. A*, 2015, **3**, 16064–16071.

40 K. Zhang, D. Kopetzki, P. H. Seeberger, M. Antonietti and F. Vilela, *Angew. Chem., Int. Ed.*, 2013, **52**, 1432–1436.

41 X. Liu, Y. Xu and D. Jiang, *J. Am. Chem. Soc.*, 2012, **134**, 8738–8741.

42 J.-X. Jiang, A. Trewin, D. J. Adams and A. I. Cooper, *Chem. Sci.*, 2011, **2**, 1777–1781.

43 Y. Xu, L. Chen, Z. Guo, A. Nagai and D. Jiang, *J. Am. Chem. Soc.*, 2011, **133**, 17622–17625.

44 H. Bohra, P. Li, C. Yang, Y. Zhao and M. Wang, *Polym. Chem.*, 2018, **9**, 1972–1982.

45 S. Hayashi, Y. Togawa, S.-I. Yamamoto, T. Koizumi, K. Nishi and A. Asano, *J. Polym. Sci., Part A: Polym. Chem.*, 2017, **55**, 3862–3867.

46 A. Alam, S. Mishra, A. Hassan, R. Bera, S. Dutta, K. Das Saha and N. Das, *ACS Omega*, 2020, **5**, 4250–4260.

47 T. Geng, W. Zhang, Z. Zhu, G. Chen, L. Ma, S. Ye and Q. Niu, *Polym. Chem.*, 2018, **9**, 777–784.

48 Z. Guo, P. Sun, X. Zhang, J. Lin, T. Shi, S. Liu, A. Sun and Z. Li, *Chem. – Asian J.*, 2018, **13**, 2046–2053.

49 S. Bai, Q. Hu, Q. Zeng, M. Wang and L. Wang, *ACS Appl. Mater. Interfaces*, 2018, **10**, 11319–11327.

50 X. Ding and B.-H. Han, *Angew. Chem., Int. Ed.*, 2015, **54**, 6536–6539.

51 Z. J. Wang, R. Li, K. Landfester and K. A. I. Zhang, *Polymer*, 2017, **126**, 291–295.

52 Y. Wei, W. Chen, X. Zhao, S. Ding, S. Han and L. Chen, *Polym. Chem.*, 2016, **7**, 3983–3988.

53 BP Statistical Review of World Energy, Report https://www.bp.com/en/global/corporate/energy-economics/statistical-review-of-world-energy.html, British Petroleum, 2019.

54 M. Stephenson, *Energy and Climate Change: An Introduction to Geological Controls, Interventions and Mitigations*, 2018, ISBN: 978-0-12-812021-7.

55 B. Zohuri, in *Nuclear Reactor Technology Development and Utilization*, ed. S. U.-D. Khan and A. Nakhabov, Woodhead Publishing, 2020, pp. 61–120, DOI: 10.1016/B978-0-12-818483-7.00002-0.

56 S. Chu and A. Majumdar, *Nature*, 2012, **488**, 294–303.

57 H. Guan, D. Zou, H. Yu, M. Liu, Z. Liu, W. Sun, F. Xu and Y. Li, *Front. Mater.*, 2019, **6**, 12.

58 H. Ma, J.-J. Chen, L. Tan, J.-H. Bu, Y. Zhu, B. Tan and A. C. Zhang, *ACS Macro Lett.*, 2016, **5**, 1039–1043.

59 N. Baig, S. Shetty, S. Al-Mousawi and B. Alameddine, *Polym. Chem.*, 2020, **11**, 3066–3074.

60 M. Janeta, W. Bury and S. Szafert, *ACS Appl. Mater. Interfaces*, 2018, **10**, 19964–19973.

61 D. Chen, Y. Fu, W. Wu, G. Yu and C. Pan, *Chem. Eng. J.*, 2018, **334**, 900–906.

62 C. Pei, T. Ben, S. Xu and S. Qiu, *J. Mater. Chem. A*, 2014, **2**, 7179–7187.

63 A. Narula and C. P. Rao, *ACS Omega*, 2019, **4**, 5731–5740.

64 M. Yan, Y. Wu, Y. Yan, X. Yan, F. Zhu, Y. Hua and W. Shi, *ACS Sustainable Chem. Eng.*, 2016, **4**, 757–766.

65 A. Kumar and S. Priyanka, *New J. Chem.*, 2019, **43**, 14997–15013.

66 L. Cheng, M. Wei, L. Huang, F. Pan, D. Xia, X. Li and A. Xu, *Ind. Eng. Chem. Res.*, 2014, **53**, 3478–3485.

67 S. Jain, S. Mishra and T. K. Sarma, *ACS Sustainable Chem. Eng.*, 2018, **6**, 9771–9783.

68 J. Lin, F. Lin, X. Chen, W. Ye, X. Li, H. Zeng and B. Van der Bruggen, *Ind. Eng. Chem. Res.*, 2019, **58**, 11003–11012.

69 G. Han, T.-S. Chung, M. Weber and C. Maletzko, *Environ. Sci. Technol.*, 2018, **52**, 3676–3684.

70 H. Liu and H. Liu, *J. Mater. Chem. A*, 2017, **5**, 9156–9162.

71 H. Liu, R. Sun, S. Feng, D. Wang and H. Liu, *Chem. Eng. J.*, 2019, **359**, 436–445.

72 D. Lehnherr, J. M. Alzola, E. B. Lobkovsky and W. R. Dichtel, *Chem. – Eur. J.*, 2015, **21**, 18122–18127.

73 X. Yang, L. Yuan, Z. Chen, Z. Liu and Q. Miao, *Org. Lett.*, 2018, **20**, 6952–6956.

74 S. J. Hein, D. Lehnherr, H. Arslan, F. J. Uribe-Romo and W. R. Dichtel, *Acc. Chem. Res.*, 2017, **50**, 2776–2788.

75 Z. Zhu and T. M. Swager, *Org. Lett.*, 2001, **3**, 3471–3474.

76 B. Alameddine, N. Baig, S. Shetty, F. Al-Sagheer and S. Al-Mousawi, *Asian J. Org. Chem.*, 2018, **7**, 378–382.

77 N. Baig, S. Shetty, S. Al-Mousawi, F. Al-Sagheer and B. Alameddine, *React. Funct. Polym.*, 2019, **139**, 153–161.

78 Z. Xie, B. Yang, L. Liu, M. Li, D. Lin, Y. Ma, G. Cheng and S. Liu, *J. Phys. Org. Chem.*, 2005, **18**, 962–973.

79 B. Alameddine, N. Baig, S. Shetty, S. Al-Mousawi and F. Al-Sagheer, *Polymer*, 2018, **154**, 233–240.

80 Y. H. Abdelmoaty, T.-D. Tessema, F. A. Choudhury, O. M. El-Kadri and H. M. El-Kaderi, *ACS Appl. Mater. Interfaces*, 2018, **10**, 16049–16058.

81 X. Qian, Z.-Q. Zhu, H.-X. Sun, F. Ren, P. Mu, W. Liang, L. Chen and A. Li, *ACS Appl. Mater. Interfaces*, 2016, **8**, 21063–21069.

82 R. M. Weiss, A. L. Short and T. Y. Meyer, *ACS Macro Lett.*, 2015, **4**, 1039–1043.

83 D. Shetty, T. Skorjanc, J. Raya, S. K. Sharma, I. Jahovic, K. Polychronopoulou, Z. Asfari, D. S. Han, S. Dewage, J.-C. Olsen, R. Jagannathan, S. Kirmizialtin and A. Trabolsi, *ACS Appl. Mater. Interfaces*, 2018, **10**, 17359–17365.

84 K. C. Park, J. Cho and C. Y. Lee, *RSC Adv.*, 2016, **6**, 75478–75481.